RSC Advances

This is an *Accepted Manuscript*, which has been through the Royal Society of Chemistry peer review process and has been accepted for publication.

Accepted Manuscripts are published online shortly after acceptance, before technical editing, formatting and proof reading. Using this free service, authors can make their results available to the community, in citable form, before we publish the edited article. This *Accepted Manuscript* will be replaced by the edited, formatted and paginated article as soon as this is available.

You can find more information about *Accepted Manuscripts* in the Information for Authors.

Please note that technical editing may introduce minor changes to the text and/or graphics, which may alter content. The journal's standard Terms & Conditions and the Ethical guidelines still apply. In no event shall the Royal Society of Chemistry be held responsible for any errors or omissions in this *Accepted Manuscript* or any consequences arising from the use of any information it contains.

ROYAL SOCIETY OF CHEMISTRY

www.rsc.org/advances

A Simple and Template Free Synthesis of Branched ZnO Nanoarchitectures for Sensor Applications

Ganesh Kumar Mani and John Bosco Balaguru Rayappan*

Centre for Nano Technology & Advanced Biomaterials (CeNTAB) and

School of Electrical & Electronics Engineering (SEEE)

SASTRA University, Thanjavur 613 401, Tamil Nadu, India.

RSC Advances Accepted Manuscript

---

*Corresponding Author

Prof. John Bosco Balaguru Rayappan, Ph.D.

Centre for Nanotechnology & Advanced Biomaterials (CeNTAB) &

School of Electrical & Electronics Engineering

SASTRA University

Thanjavur – 613 401

India

Phone: +91 4362 264 101; Ext: 2255

Fax: +91 4362 264120

E-mail: rjbosco@ece.sastra.edu (John Bosco Balaguru Rayappan)

ganesh@eee.sastra.edu (Ganesh Kumar Mani)

Abstract

Strong electrophilic natured acetaldehyde in various food and beverages damages the genetic materials and induces diseases like atherosclerosis. Detection and quantification of such carcinogen poses a major challenge. In this context, a novel room temperature acetaldehyde sensor made up of hierarchical ZnO nanostructures prepared by simple and template free method has been reported. ZnO nanostructures were grown on glass substrates by chemical spray pyrolysis technique at the substrate temperature of 523 K. Different nanostructures namely tiny nanoplatelets, branched nanorods and thicker nanoplatelets were formed by annealing process. The crystal structure, morphology, optical absorbance of the hierarchical ZnO nanostructures were investigated by X-ray diffraction (XRD), filed emission scanning electron microscope (FE-SEM), UV-vis spectrophotometer respectively. The branched nanorods showed an excellent sensing response towards 20 to 500 ppm of acetaldehyde vapour. The role of high density junctions of the branched ZnO architecture in enhancing the vapour sensing performance has been highlighted. The observed selectivity, range of detection and stability of the branched ZnO nanorods has proved it as a potential sensing element for the detection of acetaldehyde.

Keywords: ZnO, Spray Pyrolysis, Thin Film, Nanostructures, Sensors, Acetaldehyde

RSC Advances Accepted Manuscript

1. Introduction

American Conference of Governmental Industrial Hygienists (ACGIH) and Environment Agency in Japan reported that the maximum permitted concentration of acetaldehyde is about only 10 and 50 ppm respectively.[1] Japan, USA and Netherlands listed acetaldehyde as hazardous air pollutants.[2] Consumers may be exposed to acetaldehyde in several ways because of its occurrence in cheese, cooked beef, chicken, oak, tobacco leaves and also commonly found in alcoholic beverages. Due to its strong electrophilic nature, it is believed to react with DNA to induce biological changes such as mutagenesis and carcinogenesis.[3] Also it reacts with low density lipoproteins (LDH) and originate the diseases such as atherosclerosis and acute alcoholic liver disease.[4] Moreover acetaldehyde can be used as a biomarker for wine, beer, yoghurt and meat quality assessment applications.[5] Hence, there is a crucial demand to explore sensors which are capable of monitoring acetaldehyde in real time environment. Detection of acetaldehyde can be performed in several ways such as colorimetric, chemiresistive, gas spectrometric, spectrofluorometric, chromatograpic, chemiluminescence, liquid chromatography and enzymatic methods.[6,7]

Due to high performance, easy operation and low cost, metal oxide based chemical sensors have been exploited for numerous applications in various fields like automotive, industrial, aerospace, medical, domestic, security and food industries.[8,9] Several metal oxides such as TiO_2, Al_2O_3, SnO_2, MoO_3, ZnO, V_2O_5, WO_3 have been employed to detect hazardous gases in room and elevated operating temperatures.[10,11] Among them, ZnO is a commonly used sensing material due to its unique catalytic, optical and electrical properties.[12–14] ZnO nanostructure with tailored shapes and sizes are often considered to improve the performance of gas sensors. Several methods have been employed to tune the sensitivity and selectivity of the materials like element doping,

RSC Advances Accepted Manuscript

functionalization with noble metals and heterostructures formation.[15–17] To date, various morphologies of ZnO have been extensively employed to fabricate gas sensors, which includes quantum dots, nanowires, nanotubes, nanoneedles, nanotubes, nanobelts, nanosheets, nanowalls, etc.[18–22]

ZnO with different nanostructured morphology has been preferred for sensing applications because of very high surface to volume ratio, grain dimension comparable to space charge region and superior stability.[23,24] Recent studies revealed that branched / networked type of special morphologies are often associated with enhanced gas sensing properties. Complex surface morphologies have received greater research interest due to their novel properties like enhanced electrical conductivity, thermal stability, catalytic properties and low cost.[25,26] Mostly seeded growth approach have been reported for the preparation of branched 1D nanostructures. The multistep preparation is a major obstacle limiting their practical applications. Also the preparation methods require costly equipment and highly skilled experts.[27–29] ZnO thin films were deposited by several methods, but spray pyrolysis technique was preferred owing to its advantages such as simplicity, large productivity, cost effectiveness and environmentally safe since water is used as solvent and requirement of no vacuum.[30–32]

Branched 1D nanostructures have been efficiently used in wide variety of applications such as solar cells, field emitters, photo detectors, supercapacitors, transparent EMI shielding, fuel cells, etc.[33] Limited works are available on gas sensor applications. Branched ZnO heterostructures were used to detect ethanol, n-butanol, NO_2, etc., at elevated operating temperatures.[34–38] Mostly gas sensors operates at higher operating temperatures, which is not beneficial for practical applications like biological and explosives environments. To our knowledge no work have been reported on room temperature detection of acetaldehyde using ZnO nanostructures. Hence in this work, a

RSC Advances Accepted Manuscript

simple and template free synthesis of branched ZnO architectures have been prepared and investigated their acetaldehyde sensing performances at room temperature.

2. Experimental section

2.1 Film deposition

The hierarchical ZnO nanostructures derived from simple chemical spray pyrolysis technique (HOLMARC, HO-TH-04, India) were deposited on glass substrates at the temperature of 523 K.[39] Various forms of nanostructures were obtained by annealing the as-deposited samples at 523, 623 and 723 K. As a first step, 0.1 M of anhydrous zinc chloride ($ZnCl_2$, Merck, Purity 99%) was dissolved in 50 mL of deionized water (Millipore, USA) and subjected to constant stirring for 1 h. Glass substrates (Blue Star, Mumbai) were ultrasonically cleaned with acetone, ethanol and deionized water. Then the substrates were positioned on the substrate heater of the spray system. Prior to spray, the prepared precursor solution was loaded into the dispenser. The precursor solution was sprayed by an atomizer on glass substrates maintained at a constant temperature of 523 K. 50 mL of precursor solution was sprayed over the substrate with the spray rate and area of 2 mL min^{-1} and 15 cm min^{-1} respectively. The substrate to nozzle distance and carrier gas pressure was fixed as 15 cm and 2 mbar respectively.

2.2 Characterization

The structural and morphological properties were studied using X-Ray Diffractometer (D8 Focus, Bruker, Germany) and Field Emission Scanning Electron Microscope (JEOL, 6701F, Japan) respectively. The optical properties of the thin films were studied using UV-Vis spectrophotometer (Perkin Elmer, Lambda 25, USA) in the wavelength range of 200 to 800 nm

RSC Advances Accepted Manuscript

with the scan rate of 50 nm min^{-1}. The water contact angle over the film surface was measured using Contact Angle (CA) Goniometer (ramé-hart, Model 250, USA). Electrical and acetaldehyde sensing properties were carried out using an electrometer (Keithley 6517A).

2.3 Sensor fabrication and measurements

The room temperature (303 K and 55% RH) sensing characteristics of the ZnO nanoarchitectures was carried out in a sealed testing chamber of 5 L capacity endowed with gas inlet and outlet valves. The Ohmic contacts were established on the surface of the sensing element of area 10 mm × 10 mm using zero resistance copper wire and highly conducting silver paste.[40,41] The two electrodes were separated by 5 mm distance. The complete sensing set up and precise geometry of the electrical contacts can be found in our previous work.[41] Resistance of the sensing elements were continuously monitored by two probe method using high resistance electrometer (Keithley 6517A). Desired concentration of acetaldehyde was injected using microliter syringe through septum provision in the sealed chamber. The concentration of the target vapour[42] in the testing chamber was fixed using Eq. 1.

$$C_{ppm} = \frac{\delta \times V_r \times R \times T}{M \times P_b \times V_b} \quad -----(1)$$

where, δ is the density of acetaldehyde, V_r is the volume of acetaldehyde injected, R is the universal gas constant, T is the absolute temperature, M is the molecular weight, P_b is the pressure inside the chamber and V_b is the volume of the chamber. The sensor response (S) was calculated using the relation R_a / R_g where, R_a and R_g are the resistance of the sensing elements is in air and target gas. Since as-deposited films showed an unstable base resistance in air atmosphere, annealed films alone were considered for sensing studies. All the sensing measurements were done at room temperature.

RSC Advances Accepted Manuscript

3. Results and discussion

3.1 Morphological studies

Fig. 1 shows the formation of ZnO thin films at the substrate temperature of 523 K as well as at the annealing temperatures of 523, 623 and 723 K. This scheme clearly depicts the shape transformation of as-deposited ZnO nanoplatelets (Fig. 2a) into diverse nanostructures such as tiny platelets (Fig. 2b), branched nanorods (Fig. 2c) and thicker nanoplatelets (Fig. 2d) as a function of annealing process. The as-deposited ZnO nanoplatelets were randomly connected to each other and the thickness of these nanoplatelets were found to be in the range of 110 – 130 nm. Some irregular particles were also observed along with the nanoplatelets and it could be attributed due to the presence of incomplete decomposition of chloride salt.[39] Hence, the annealing process was considered to prepare ZnO nanostructures without precursor residues. While annealing the as-deposited nanoplatelets at 523 K, tiny nanoplatelets were formed. Further increase in the annealing temperature to 623 K, the surface morphology showed the co-existence of 2D nanoplatelets with 1D nanorods. In this structure, roots of the nanorods were formed at the surface of ZnO nanoplatelets and grown outward with lengths ranging from 300 to 330 nm and filled the intervals between the nanoplatelets. At 723 K, the nanoplatelets became denser and thicker with shorter nanorods than formed at 623 K.

3.2 Formation mechanism

Based on the observed results, the growth process of ZnO nanoarchitectures has been proposed. Generally, structure directing or capping agents such as sodium dodecyl sulfate, cetyltrimethylammonium bromide, thiourea, thiocarbamide, have been used along with precursor salts (zinc acetate, zinc nitrate and zinc chloride) to obtain various ZnO nanostructures.[43–45] Mostly

RSC Advances Accepted Manuscript

spherical morphology was achieved using zinc acetate and nitrate precursor without any structure directing agents. But zinc chloride has an inherent property of forming hexagonal rod / platelet like structure without any capping agents. Previously, Smith *et al* have extensively investigated this unique property and concluded that the byproduct formed during pyrolysis process itself acts as structure directing agent. At the pyrolysis region, the byproduct namely HCl acts as a capping or structure directing agent and it controls the growth of nuclei and hence results in various morphology.[39,46–48] The possible reaction mechanism of ZnO using zinc chloride precursor is given in Eq.2.

$$ZnCl_2 + H_2O \xrightarrow{\Delta} ZnO \uparrow + HCl \uparrow \quad -----(2)$$

ZnO formation originates from the reaction between Zn^{2+} and OH^- ions. As the precursor solution sprayed on the pre-heated substrate, ZnO was formed by the decomposition of zinc hydroxide. Firstly, thinner nanoplatelets were grown on glass substrates at the substrate temperature of 523 K with the assistance of byproducts formed during decomposition. The as-deposited film resembles with the simonkolleite ($Zn_5(OH)_8Cl_2 \cdot 2H_2O$) crystal structure. The as-deposited film was subjected to annealing to obtain complete ZnO film. In the early stage of annealing process (523 K), thinner nanoplatelets broke up into smaller units and they acted as nucleation centers for the growth of nanorods. This growth was heterogeneously occurred in both the sides of tiny nanoplatelets (Supplementary Fig. S1). But, the nanorod growth rate was limited due to the lack of thermal energy. Consequently at intermediate temperature (623 K) all the tiny nanoplatelets were converted into to smaller grains. These smaller grains acted as seeds for the growth of ZnO nanorods in lateral direction. At higher temperature (723 K), due to coalescence process, smaller grains were combined together to form bigger grains. Hence the growth of larger nanorods originated by fusing individual nanorods with each other.

RSC Advances Accepted Manuscript

3.3 Structural studies

XRD measurements (Fig. 3) were carried out to determine the crystal plane orientation and crystallite size of the as-deposited and annealed ZnO nanoplatelets. Patterns of as-deposited ZnO thin films showed a relatively low intensity ZnO peaks and several other peaks corresponding to ZnO, Zn and ZnOH. It might be due to the incomplete decomposition of precursor salt which resembles with the crystal structure of simonkolleite $Zn_5(OH)_8Cl_2 \cdot 2H_2O$) (JCPDS 07-0155).[49] The annealed films showed a dominant (002) crystal plane orientation which indicated that the films were preferably oriented along *c* axis and well matched with JCPDS card No: 36-1451. The average crystallite sizes of the ZnO thin films were estimated with reference to (002) plane using Scherrer's formula[21] and found to be 33, 36 and 38 nm for tiny nanoplatelets, branched nanorods and thicker nanorods respectively.

3.4 Optical studies

Fig. 4 shows the optical absorbance spectra of the films in the wavelength range of 350 to 800 nm. The major difference in absorbance values of the three different nanoarchitectures can be primarily attributed to scattering of incident light at the grain boundaries. In the case of tiny nanoplatelets, presence of higher surface coverage with lesser voids captures as well as traps the incident light to a maximum extent. The absorption was further increased by multiple reflection effect when light interacts with tiny nanoplatelets and branched nanorods which in-turn extends the spatial and temporal light absorption.[50] But in the case of thinner and thicker nanoplatelets the lower surface coverage and large number of open voids facilitates lesser absorption of incident light. In other words, surface filling factor and branched architectures play an important role in determining the light absorption through multiple scattering.

RSC Advances Accepted Manuscript

3.5 Wettability studies

The contact angle (CA) between water and film surface determines the wettability nature of the surface whether it is hydrophilic (< 90°) or hydrophobic (> 90°).[51] Fig. 5 shows the water wettability properties of the as-deposited and annealed ZnO thin films. As-deposited film exhibited CA of about 80°. Except this case, all other annealed ZnO thin films showed a hydrophobic nature. The obtained results are well consistent with the morphological studies. As-deposited film surface showed a hexagonal shaped ZnO platelets with smooth surface (relatively low roughness), which revealed the hydrophilic nature. Once the film was subjected to annealing treatment, the change in morphology namely tiny nanoplatelets, branched nanorods and denser nanoplatelets resulted in the increased surface roughness. Film with higher surface roughness traps more air pockets beneath the water drop and hence the contact angle increases.[52] The film annealed at 623 K showed quite different morphology and displayed high CA of about 134°. Admittedly, these results proved that annealing can effectively change the wettability nature of the thin film.

3.6 Sensing studies

3.6.1 Selectivity

Selectivity of the sensing element can be defined as, the capability of sensor to response specific gases than others. In fact, highly selective sensor can be used to detect the specific gas/vapour when it is exposed to a multicomponent gas/vapour environment. Therefore the response of the ZnO nanostructures was tested in the presence of 100 ppm of various vapours namely ammonia, acetone, ethanol, methanol, formaldehyde, toluene and acetaldehyde. Fig. 6 a,b summarizes the sensing responses of the three sensing elements toward the test vapours. Surprisingly, all the three different nanostructures showed a high response towards acetaldehyde

RSC Advances Accepted Manuscript

vapour. Meanwhile responses to other vapours were not exceeded 13. The branched nanorods showed a remarkable response which was around 16 and 4 times higher than that of tiny and thicker nanoplatelets respectively. Noticeably, these sensor elements showed a considerable response to formaldehyde. Selectivity towards acetaldehyde might be due to the lesser dissociation energy of it (364 kJ mol^{-1}) than other vapours namely ammonia (435 kJ mol^{-1}), acetone (393 kJ mol^{-1}), ethanol (436 kJ mol^{-1}), formaldehyde (364 kJ mol^{-1}) and toluene (368 kJ mol^{-1}). Even though the dissociation energy of acetaldehyde and formaldehyde are same, the number of electrons released during sorption process made acetaldehyde more sensitive than formaldehyde.[39]

3.6.2 Transient and response studies

Herein, we studied the room temperature sensing response of the three different morphologies toward various concentrations of acetaldehyde. The transient response recovery characteristics are shown in Fig. 7a. The fall in resistance within few seconds was observed when injecting the reducing type target vapour inside the chamber indicated the n-type semiconductor behaviour of the sensing element.[53] All the films recovered to baseline value once the target vapour was exhausted. It was also obvious that as the concentration of target vapour increased, the response amplitude was also increased. Some fluctuations were observed in the readings and it might be due to the turbulences at the ambient around the sensor. The lowest detection limit was varied as 50 ppm, 20 ppm and 5 ppm for tiny nanoplatelets, branched nanorods and thicker nanoplatelets respectively.

On the basis of data collected upon sequence exposure of acetaldehyde at different concentrations, the response curves are shown in Fig. 7b. The response values for 100 ppm of acetaldehyde were 36, 587 and 140 for tiny nanoplatelets, branched nanorods and thicker

RSC Advances Accepted Manuscript

nanoplatelets respectively. The obtained sensing response for branched nanorods was about 16 and 4 times higher than that of tiny and thicker nanoplatelets respectively. In the case of tiny nanoplatelets the response values of 4.1, 36, 72, 125.8 and 128.5 were observed for 50, 100, 250, 500 and 1000 ppm of acetaldehyde respectively. The response over 50 ppm becomes more or less saturated in the case of tiny nanoplatelets. The sensing response of branched nanorods were 2.8, 3.6, 66, 92, 587, 3083 and 7872 for 20, 30, 50, 75, 100, 250 and 500 ppm of acetaldehyde respectively. Interestingly, it showed 4 order magnitude change ($4.7 \times 10^6\ \Omega$ for 500 ppm) with respect to its baseline resistance ($3.7 \times 10^{10}\ \Omega$). It is apparent that branched nanorods sensors showed a wide detection range of 20 ppm to 1000 ppm. Even for 5 ppm, thicker nanoplatelets showed a response of 4.3 but the sensor was saturated at 100 ppm of acetaldehyde itself. Whereas no response was recorded for lower concentrations in tiny nanoplatelets and branched nanorods.

3.6.3 Response / Recovery times

Response and recovery times are very crucial parameter for a gas sensor. The response and recovery times were calculated from time vs resistance plot, which is defined as the time taken to attain 90% and 10% of target gas resistance from its baseline resistance respectively.[41] Supplementary Fig. S2 shows the typical response recovery times of the three different sensing elements. As the concentration was increased, the response time was reduced to few seconds due to the simultaneous interaction of higher number of target molecules with the sensing element. Also the recovery time of the sensing element was constantly increased with increasing concentration due to slow desorption of target gas molecules from the surface. The response/recovery time of 116/44 (tiny nanoplatelets), 112/54 (branched nanorods) and 97/186 (thicker nanoplatelets) towards 100 ppm of acetaldehyde respectively were observed. Furthermore,

RSC Advances Accepted Manuscript

branched nanorods showed a very fast recovery of 7 s for 20 ppm of acetaldehyde. Also reproducibility of the branched nanorods were checked for five times towards 100 ppm of acetaldehyde and it showed a fair reproducibility behaviour. The reason behind the excellent selectivity, high sensitivity and quick response, recovery times of the hierarchical nanostructures was explained in the following section.

3.6.4 Sensing mechanism

ZnO is one of the highly versatile sensing materials to detect various gases. It is well known that the surface morphology plays a significant role on determining the sensor responses of the semiconductor materials. Gas sensors are the surface-controlled types, where the dimensions, surface states and quantities of adsorbed oxygen molecules influence the sensing performance significantly. Moreover the electrical properties of one-dimensional (1D) ZnO nanostructured arrays are exceedingly sensitive to the adsorbed species, because of their high surface-to-volume ratio, which allows the surface atoms to have more opportunities to participate in the surface reactions. Compared with 1D & 2D nanostructures, 3D nanostructures facilitates to enhance the properties of the sensing material.[54–57] In particular, branched/networked type of morphologies are often associated with enhanced gas sensing properties.[34–38] Gas sensing mechanism of most metal oxide semiconductor sensors can be recognized as change in their electrical conductivity in the presence and absence of target gases.

When the hierarchical nanostructures been continuously exposed to the ambient atmosphere, the ambient oxygen adsorbed on the ZnO surface, thereby resulted in the formation of depletion layer and ultimately increased the resistance. According to the commonly accepted

RSC Advances Accepted Manuscript

Barsan and Weimar conduction model[58], the oxygen adsorption domination species depends on temperature. Hence, at room temperature O_2^- adsorption is dominant and it can be written as Eq. 3

$$O_{2\,(atmosphere)} + e^-_{(ZnO\ surface)} \longrightarrow O^-_{2\,(ZnO\ surface)} \quad ------ (3)$$

Since acetaldehyde is a reducing gas, it gets oxidized into CO_2 and H_2O while interacting with adsorbed oxygen on the ZnO surface. Hence the trapped electrons are put back in the conduction band (i.e. thinning of the space charge region thus decreasing the potential barrier) of sensing element lead to increase in conductivity. The proposed acetaldehyde sensing mechanism is given in Eq. 4,

$$2CH_3CHO + 5O_{2\,(ZnO\ surface)}^- \longrightarrow 4CO_2 \uparrow + 4H_2O \uparrow + 5e^-_{(ZnO\ surface)} \quad ------ (4)$$

In order to validate the proposed sensing mechanism, a simple lime water test was carried out and described in detail in our previous work.[39]

In summary, branched nanorod morphology showed the maximum response. Fig. 8a-d shows the highlighted view of the branched nanorod morphologies. It clearly shows that branched nanorods roots (Fig. 8a) from backbone of tiny grains and grown around 300 nm in length. The sensor with branched nanorods provides more pathways such as stem made up of tiny grains (Fig. 8b) ranging from 40 to 60 nm, networked nanorods length around 300 nm (Fig. 8c) to electron exchange during gas interaction. Also the tip (Fig. 8d) of the nanorods showed the hexagonal morphology. The large amount of open space between nanorods is also be highly beneficial for the diffusion of gases which might have enhanced the sensing performance. At higher concentrations, the high sensing response of 3083 and 7872 for 250 and 500 ppm concentration was observed. It might be due to the switching from a highly non-activated into activated state of the entire hierarchical branched nanowires at higher concentrations. Generally crystallinity of the materials is often associated with sensing performance. When crystallinity increases, the intrinsic resistance of the material

RSC Advances Accepted Manuscript

decreases.[59,60] The obtained resistance values for the three different nanoarchitectures (tiny nanoplatelets, branched nanorods and thicker nanoplatelets) are 1.8×10^{11}, 3.7×10^{10} and 1.8×10^{11} Ω. Among them, branched nanorods with better crystallinity showed lower resistance which indicates the significantly improved electron transport between stem-rods and consequently resulted in the high sensing performance.

Though the tiny and thicker nanoplatelets possessed more open space than branched nanorods, the presence of both the large active area (rods & stems) and open space made the branched nanorod more sensitive than the other structures. The calculated responses were found to be 36 and 139.7 for 100 ppm of acetaldehyde for tiny and thicker nanoplatelets respectively. To understand the enhanced response of thicker nanoplatelets, the morphology was further examined and highlighted view is shown in Fig. 8e. The highlighted view elucidates the laterally grown nanorods with larger diameter from the stems which might be the reason for the better response of thicker nanoplatelets than that of tiny.

To precise the sensing mechanism, the schematic of the three different morphologies are depicted in Fig. 9. J_{Total} is referred as the number of junctions in the film morphology. Tiny nanoplatelets showed only one kind of junction namely intergranular contacts in stem (J_1). Thicker nanoplatelets showed an additional type of junction between inter-granular and nanorods (J_2). But, branched nanorods possessed four different junctions namely intergranular contacts in stem (J_1), intergranular-nanorod (J_2), nanorod-nanorod (J_3) and intergranular contacts in nanorods (J_4). The surface depletion region of individual nanorods and high potential barriers created in junctions facilitate 2-fold superior sensitivity than other nanostructures. In literature, Park *et al* systematically studied the density of the junctions in networked SnO_2 nanowires and their sensing properties. They have reported that the sensing performance was outstanding for films with

RSC Advances Accepted Manuscript

morphology of high density junctions.[61] Also the effect of humidity on the sensing response of ZnO nanoarchitectures was studied towards 100 ppm of acetaldehyde and is shown in Fig. 10. At lower humidity levels, due to less number of adsorbed OH ions on the ZnO surface, availability of more active sites for gas solid interaction resulted in better response. At higher humidity levels, the response was reduced due to the inhibition of active sites on the ZnO surface by the OH ions as expected.[40,42] The co-efficient of variation of sensing response for tiny nanoplatelets, branched nanorods and thicker nanoplatelets was found to be 44%, 6% and 14% respectively with reference to various humidity levels. These results can be correlated with the measured contact angle values. The obtained contact angles are in the following order: branched nanorods (CA=134^{o}) ≤ thicker nanoplatelets (CA=119^{o}) ≤ tiny nanoplatelets (CA=91^{o}). Since nanostructures with large contact angle is of more hydrophobic, it does not allow OH ions to be adsorbed on the surface. Hence, film with branched nanorod architecture showed less co-efficient of variation in its sensing response at various humidity levels.

Compared with the previous reports on ZnO acetaldehyde sensors, Calestini *et al* achieved the response of 47.5 for 50 ppm using ZnO tetrapods at the operating temperature of 400^{o}C.[24] Gilbeti *et al* studied the acetaldehyde detection using ZnO powders prepared by sol gel technique and reported the sensor performance but limited to 10 ppm concentration at the operating temperature of 450^{o}C.[62] Similarly Rai *et al* prepared ZnO nanorods using microwave assisted hydrothermal method and achieved the highest response of 5.30 for 250 ppm at 400^{o}C.[63] Recently Zhang *et al* discussed the acetaldehyde sensing performance of ZnO nanosheets and reported the response of ~ 80 for 1 ppm at 220^{o}C.[64] All these reports signifies the ZnO sensor performance at the elevated operating temperatures. But the present work highlights the advantages of room temperature sensing, wide detection range and simple fabrication procedure, cost effective

RSC Advances Accepted Manuscript

synthesis routes of ZnO sensing element. Therefore, ZnO nanostructure with multiple junctions has been identified as a promising candidate to detect acetaldehyde at room temperature.

4. Conclusion

In conclusion, through annealing treatment of spray deposited ZnO thin film, various hierarchical nanostructures like tiny nanoplatelets, branched nanorods and thicker nanoplatelets were formed. The first implementation of branched ZnO nanorods as room temperature acetaldehyde sensor has been successfully accomplished. The branched nanorod structure provided the response of 587 for 100 ppm of acetaldehyde with the response and recovery times of 112 and 54 s, respectively. Combined morphology like nanorod roots from nanoplatelets were able to generate more active centers for interaction with gas molecules and hence increased the sensing response. Under similar test conditions tiny and thicker nanoplatelets showed low response with narrow range of detection. These results demonstrated that the hierarchical ZnO nanostructures can be used to fabricate low power, cost effective acetaldehyde sensor with better figure of merit.

RSC Advances Accepted Manuscript

Acknowledgements

The authors wish to express their sincere thanks to the Department of Science & Technology, New Delhi, India for the financial support (Project ID: INT/SWD/VINN/P-04/2011 & SR/FST/ETI-284/2011(C)). They also wish to acknowledge SASTRA University, Thanjavur for extending infrastructure support to carry out this work.

RSC Advances Accepted Manuscript

Figure Captions

Fig. 1 Synthesis strategy to hierarchical ZnO nanostructures.

Fig. 2 FESEM images of a) larger nanoplatelets, b) tiny nanoplatelets, c) branched nanorods and d) thicker nanoplatelets.

Fig. 3 XRD patterns of hierarchical ZnO nanostructures.

Fig. 4 Absorbance spectra of hierarchical ZnO nanostructures.

Fig. 5 Wettability nature of various ZnO nanostructures.

Fig. 6 a) Selectivity nature of the sensing element and b) highlighted view of the low sensing response.

Fig. 7 a) Transient resistance response and b) response trend of various ZnO nanostructures.

Fig. 8 High magnification FESEM image of a) branched nanorods, b) stem of branched nanorods, c) complete view of nanorods, d) tip of hexagonal nanorods and e) thicker nanoplatelets.

Fig. 9 Schematic diagram showing the density of junctions in hierarchical nanostructures. Potential barrier built up in J1) intergranular contacts, J2) between inter-granular and nanorods, J3) nanorod-nanorod and J4) intergranular contacts in nanorods.

Fig. 10 Response towards 100 ppm of acetaldehyde with respect to various humidity levels.

RSC Advances Accepted Manuscript

References

1. K. Mitsubayashi, H. Amagai, H. Watanabe, and Y. Nakayama, *Sensors Actuators B Chem.*, 2003, **95**, 303–308.
2. E. Przyk, A. Świtaj-Zawadka, P. Konieczka, J. Szczygelska-Tao, J. F. Biernat, and J. Namieśnik, *Anal. Chim. Acta*, 2003, **488**, 89–96.
3. M. E. Ghica, R. Pauliukaite, N. Marchand, E. Devic, and C. M. A. Brett, *Anal. Chim. Acta*, 2007, **591**, 80–86.
4. T. Miyake and T. Shibamoto, *J. Chromatogr. B. Biomed. Sci. Appl.*, 1998, **719**, 213–216.
5. A. Avramescu, T. Noguer, M. Avramescu, and J.-L. Marty, *Anal. Chim. Acta*, 2002, **458**, 203–213.
6. A. a Mohamed, A. T. Mubarak, Z. M. H. Marestani, and K. F. Fawy, *Talanta*, 2008, **74**, 578–585.
7. W. Ma and W. R. Klemm, *Alcohol*, 1997, **14**, 469–472.
8. N. Ramgir, N. Datta, M. Kaur, S. Kailasaganapathi, A. K. Debnath, D. K. Aswal, and S. K. Gupta, *Colloids Surfaces A Physicochem. Eng. Asp.*, 2013, **439**, 101–116.
9. Y.-B. Hahn, R. Ahmad, and N. Tripathy, *Chem. Commun.*, 2012, **48**, 10369–10385.
10. X. Liu, S. Cheng, H. Liu, S. Hu, D. Zhang, and H. Ning, *Sensors*, 2012, **12**, 9635–9665.
11. R. Boppella, P. Manjula, S. Arunkumar, and S. V Manorama, *Chem. Sensors*, 2014, **4**, 1–22.
12. A. Wei, L. Pan, and W. Huang, *Mater. Sci. Eng. B*, 2011, **176**, 1409–1421.
13. J. Kennedy, P. P. Murmu, E. Manikandan, and S. Y. Lee, *J. Alloys Compd.*, 2014, **616**, 614–617.

RSC Advances Accepted Manuscript

14. F. Fang, J. Futter, A. Markwitz, and J. V. Kennedy, *Mater. Sci. Forum*, 2012, **700**, 150–153.

15. C. Zhao, G. Zhang, W. Han, J. Fu, Y. He, Z. Zhang, and E. Xie, *CrystEngComm*, 2013, **15**, 6491.

16. S. Wang, Z. Li, P. Wang, C. Xiao, R. Zhao, B. Xiao, T. Yang, and M. Zhang, *CrystEngComm*, 2014, **16**, 5716.

17. F. Fang, J. Futter, A. Markwitz, and J. Kennedy, *Nanotechnology*, 2009, **20**, 245502.

18. J. Huang and Q. Wan, *Sensors*, 2009, **9**, 9903–24.

19. J. H. Lee, *Sensors Actuators B Chem.*, 2009, **140**, 319–336.

20. G.-C. Yi, C. Wang, and W. Il Park, *Semicond. Sci. Technol.*, 2005, **20**, S22–S34.

21. K. Sivalingam, P. Shankar, G. K. Mani, and J. B. B. Rayappan, *Mater. Lett.*, 2014, **134**, 47–50.

22. E. Gunasekaran, P. Shankar, G. K. Mani, and J. B. B. Rayappan, *Eur. Phys. J. - Appl. Phys.*, 2014, **67**, 20301 (1–7).

23. A. Gurlo, *Nanoscale*, 2011, **3**, 154–165.

24. D. Calestani, R. Mosca, M. Zanichelli, M. Villani, and A. Zappettini, *J. Mater. Chem.*, 2011, **21**, 15532.

25. Z. Lou, F. Li, J. Deng, L. Wang, and T. Zhang, *ACS Appl. Mater. Interfaces*, 2013, **5**, 12310–12316.

26. Y. Liu, Y. Jiao, Z. Zhang, F. Qu, A. Umar, and X. Wu, *ACS Appl. Mater. Interfaces*, 2014, **6**, 2174–2184.

27. S. Sarkar and D. Basak, *Sensors Actuators B Chem.*, 2013, **176**, 374–378.

28. S. An, S. Park, H. Ko, C. Jin, W. I. Lee, and C. Lee, *Thin Solid Films*, 2013, **547**, 241–245.

RSC Advances Accepted Manuscript

29. J. Liu, W. Wu, S. Bai, and Y. Qin, *ACS Appl. Mater. Interfaces*, 2011, **3**, 4197–4200.

30. P. S. Patil, *Mater. Chem. Phys.*, 1999, **59**, 185–198.

31. J. Mooney, B, and S. B. Radding, *Annu. Rev. Mater. Sci.*, 1982, **12**, 81–101.

32. D. Perednis and L. J. Gauckler, *J. Electroceramics*, 2005, **14**, 103–111.

33. J. Y. Lao, J. G. Wen, and Z. F. Ren, *Nano Lett.*, 2002, **2**, 1287–1291.

34. H.-U. Lee, K. Ahn, S.-J. Lee, J.-P. Kim, H.-G. Kim, S.-Y. Jeong, and C.-R. Cho, *Appl. Phys. Lett.*, 2011, **98**, 193114.

35. Y. Zhang, J. Xu, Q. Xiang, H. Li, Q. Pan, and P. Xu, *J. Phys. Chem. C*, 2009, **113**, 3430–3435.

36. J. Zhang, S. Wang, M. Xu, Y. Wang, B. Zhu, S. Zhang, W. Huang, and S. Wu, *Cryst. Growth Des.*, 2009, **9**, 3532–3537.

37. M.-W. Ahn, K.-S. Park, J.-H. Heo, D.-W. Kim, K. J. Choi, and J.-G. Park, *Sensors Actuators B Chem.*, 2009, **138**, 168–173.

38. S.-W. Choi, A. Katoch, G.-J. Sun, and S. S. Kim, *Sensors Actuators B Chem.*, 2013, **181**, 787–794.

39. G. K. Mani and J. B. B. Rayappan, *Sensors Actuators B Chem.*, 2014, **198**, 125–133.

40. G. K. Mani and J. B. B. Rayappan, *Sensors Actuators B Chem.*, 2013, **183**, 459–466.

41. G. K. Mani and J. B. B. Rayappan, *Appl. Surf. Sci.*, 2014, **311**, 405–412.

42. R. Pandeeswari and B. G. Jeyaprakash, *Sensors Actuators B Chem.*, 2014, **195**, 206–214.

43. M. Duta, D. Perniu, and a. Duta, *Appl. Surf. Sci.*, 2014, **306**, 80–88.

44. T. Dedova, O. Volobujeva, J. Klauson, A. Mere, and M. Krunks, *Nanoscale Res. Lett.*, 2007, **2**, 391–396.

RSC Advances Accepted Manuscript

45. E. Sonmez, T. Karacali, A. E. Ekinci, and M. Ertugrul, *IEEE Trans. Nanotechnol.*, 2011, **10**, 532–536.

46. A. Smith, *Thin Solid Films*, 2000, **376**, 47–55.

47. Á. Smith and R. Rodriguez-clemente, *Thin Solid Films*, 1999, **345**, 192–196.

48. A. Smith, J. Laurent, D. S. Smith, J. Bonnet, and R. Rodriguez, *Thin Solid Films*, 1995, **266**, 20–30.

49. J. Sithole, B. D. Ngom, S. Khamlich, E. Manikanadan, N. Manyala, M. L. Saboungi, D. Knoessen, R. Nemutudi, and M. Maaza, *Appl. Surf. Sci.*, 2012, **258**, 7839–7843.

50. X. Sun, Q. Li, J. Jiang, and Y. Mao, *Nanoscale*, 2014, **6**, 8769–8780.

51. Y. Yuan and T. R. Lee, *Surface Science Techniques*, Springer Berlin Heidelberg, Berlin, Heidelberg, 2013, vol. 51.

52. Y. Li, M. Zheng, L. Ma, M. Zhong, and W. Shen, *Inorg. Chem.*, 2008, **47**, 3140–3143.

53. R. L. Vander Wal, G. W. Hunter, J. C. Xu, M. J. Kulis, G. M. Berger, and T. M. Ticich, *Sensors Actuators B Chem.*, 2009, **138**, 113–119.

54. M. R. Alenezi, S. J. Henley, N. G. Emerson, and S. R. P. Silva, *Nanoscale*, 2014, **6**, 235–247.

55. A. Kolmakov and M. Moskovits, *Annu. Rev. Mater. Res.*, 2004, **34**, 151–180.

56. C. Soldano, E. Comini, C. Baratto, M. Ferroni, G. Faglia, and G. Sberveglieri, *J. Am. Ceram. Soc.*, 2012, **95**, 831–850.

57. E. Comini, C. Baratto, G. Faglia, M. Ferroni, a. Vomiero, and G. Sberveglieri, *Prog. Mater. Sci.*, 2009, **54**, 1–67.

58. N. Barsan and U. Weimar, *J. Electroceramics*, 2001, **7**, 143–167.

RSC Advances Accepted Manuscript

59. H. Xu, X. Liu, D. Cui, M. Li, and M. Jiang, *Sensors Actuators B Chem.*, 2006, **114**, 301–307.

60. Y. Lü, W. Zhan, Y. He, Y. Wang, X. Kong, Q. Kuang, Z. Xie, and L. Zheng, *ACS Appl. Mater. Interfaces*, 2014, **6**, 4186–4195.

61. J. Park, S. Choi, and S. Kim, *J. Phys. Chem. C*, 2011, **115**, 12774–12781.

62. A. Giberti, M. C. C. Carotta, B. Fabbri, S. Gherardi, V. Guidi, and C. Malagù, *Sensors Actuators B Chem.*, 2012, **174**, 402–405.

63. P. Rai, H.-M. Song, Y.-S. Kim, M.-K. Song, P.-R. Oh, J.-M. Yoon, and Y.-T. Yu, *Mater. Lett.*, 2012, **68**, 90–93.

64. S.-L. Zhang, J.-O. Lim, J.-S. Huh, J.-S. Noh, and W. Lee, *Curr. Appl. Phys.*, 2013, **13**, S156–S161.

RSC Advances Accepted Manuscript

Fig. 1

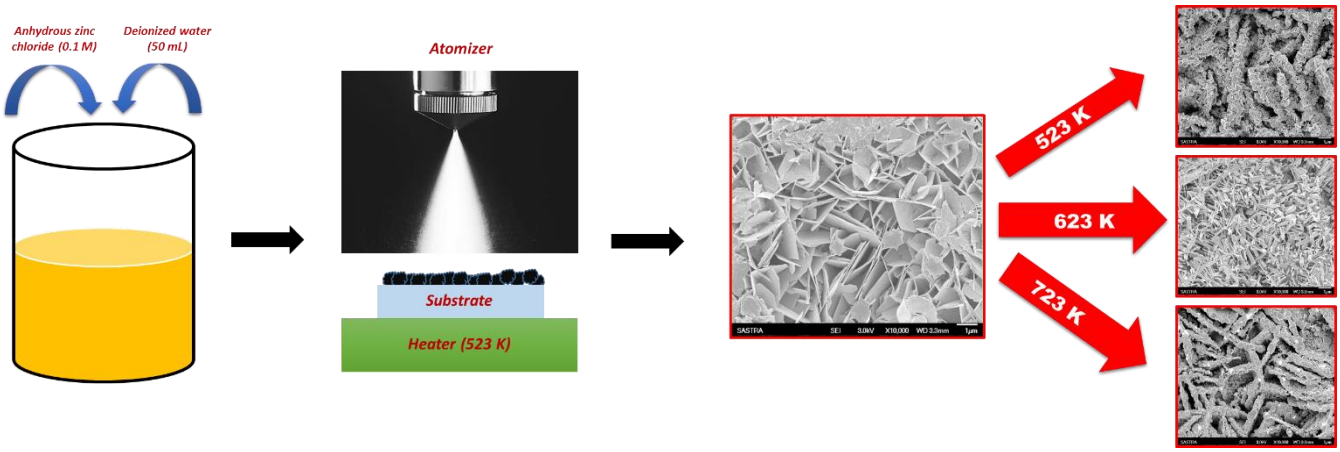

RSC Advances Accepted Manuscript

Fig. 2

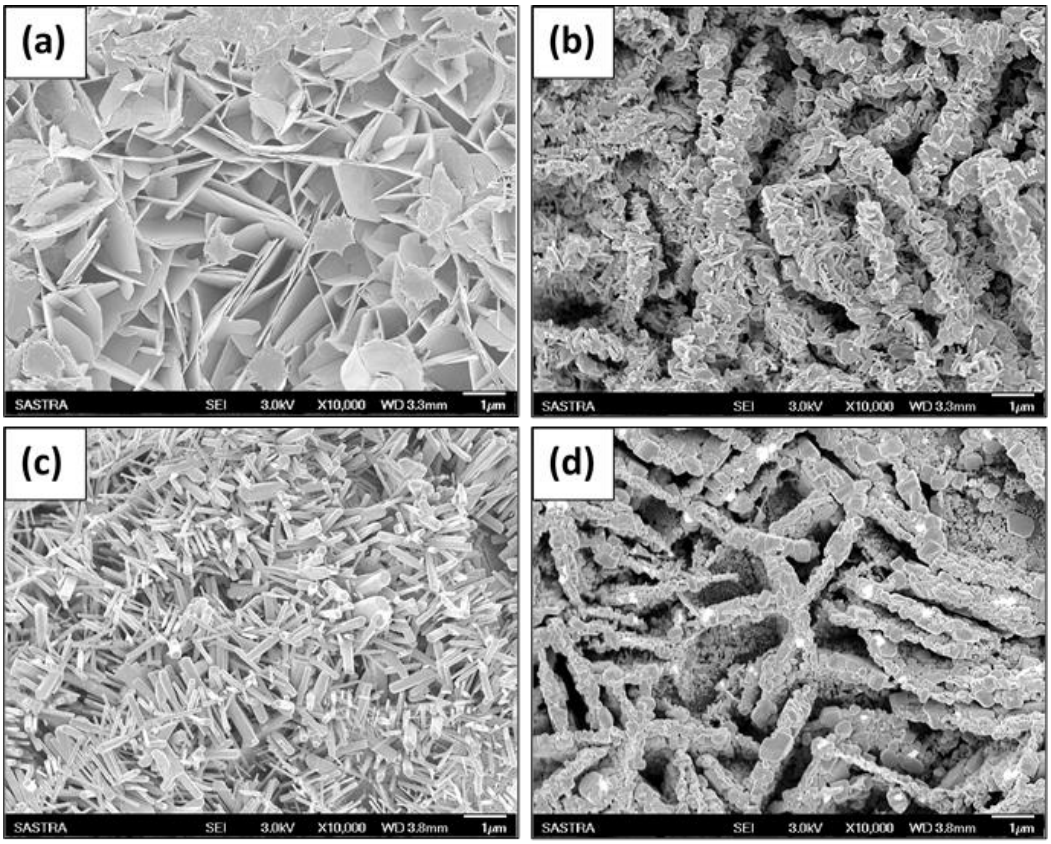

RSC Advances Accepted Manuscript

Fig. 3

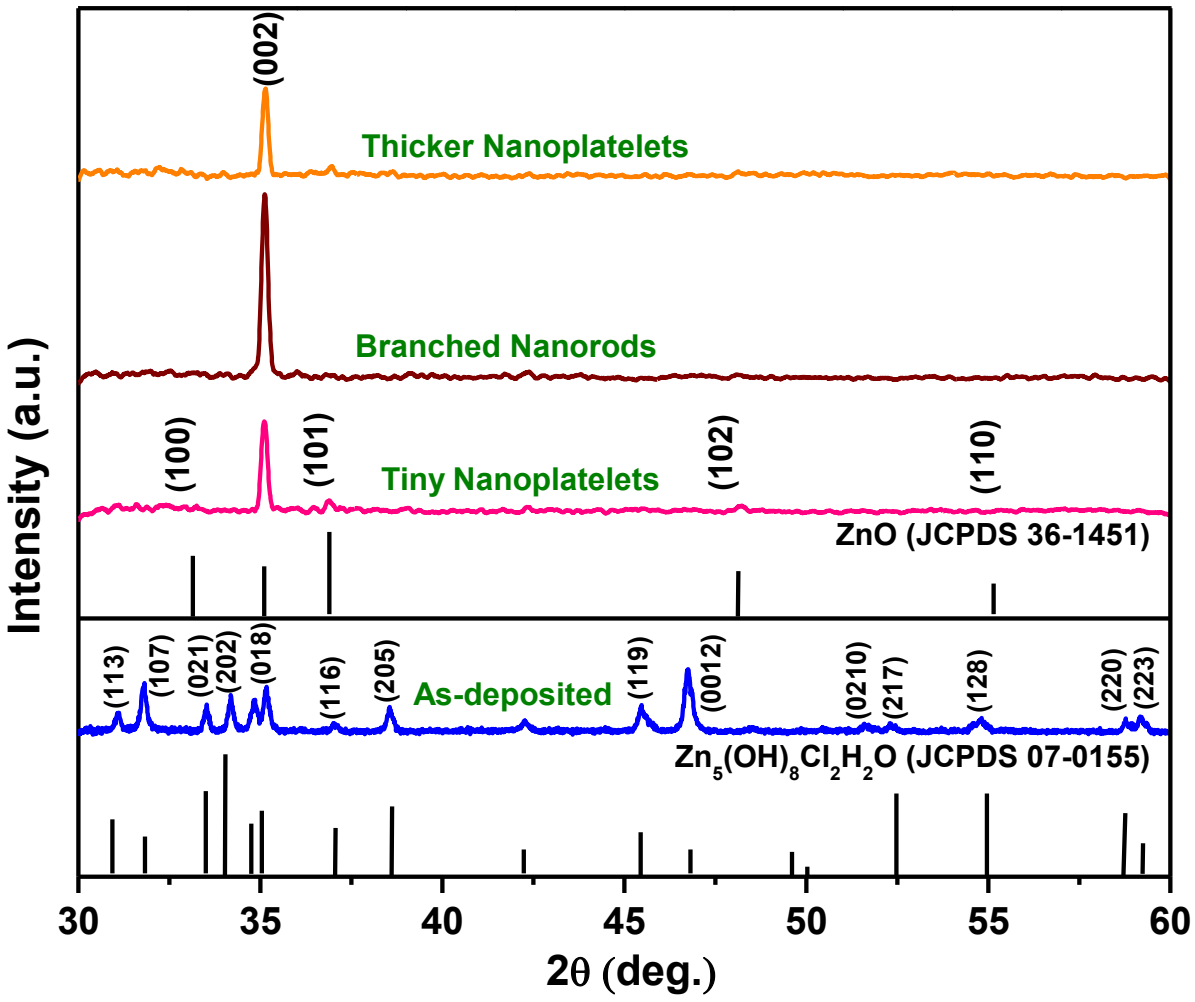

RSC Advances Accepted Manuscript

Fig. 4

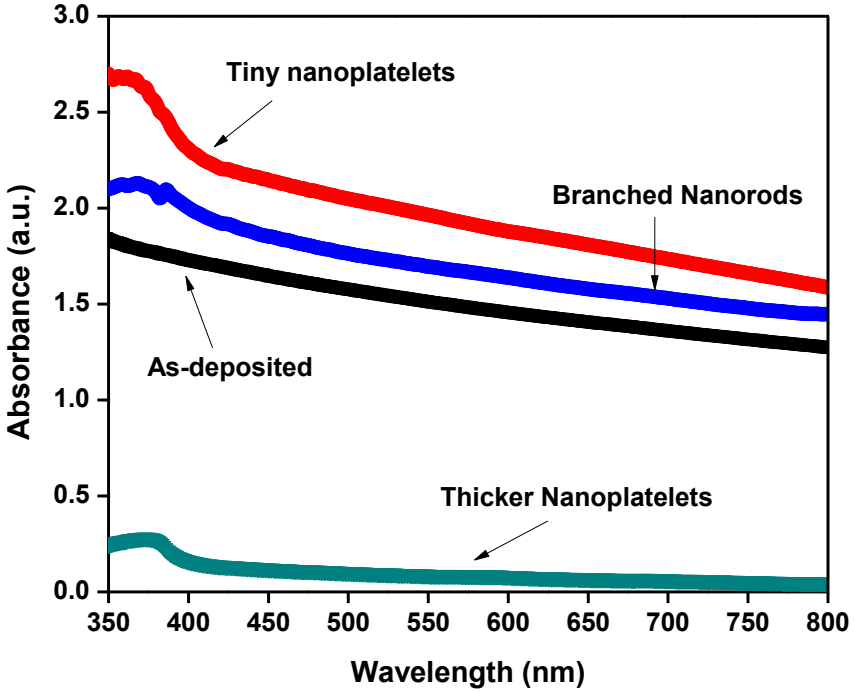

RSC Advances Accepted Manuscript

Fig. 5

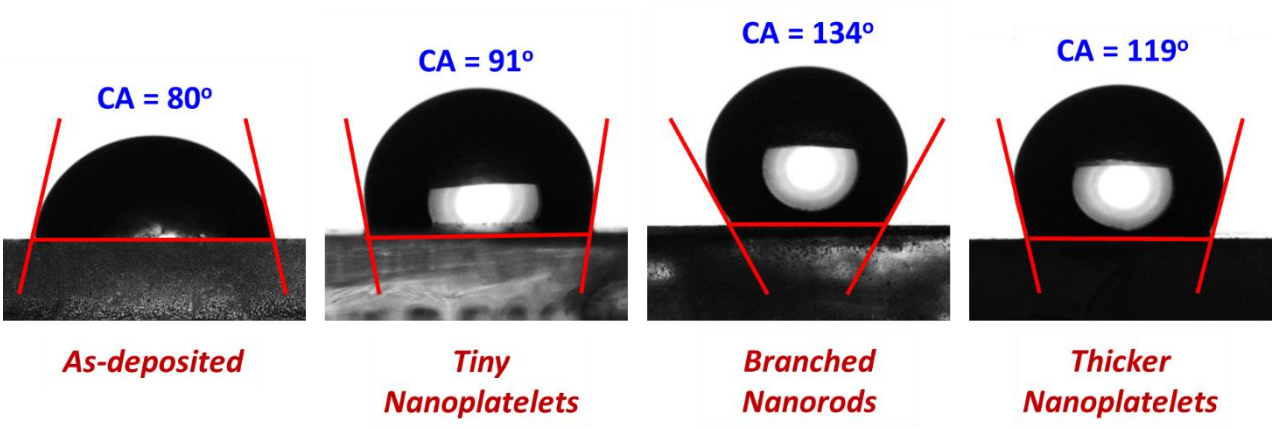

RSC Advances Accepted Manuscript

Fig. 6

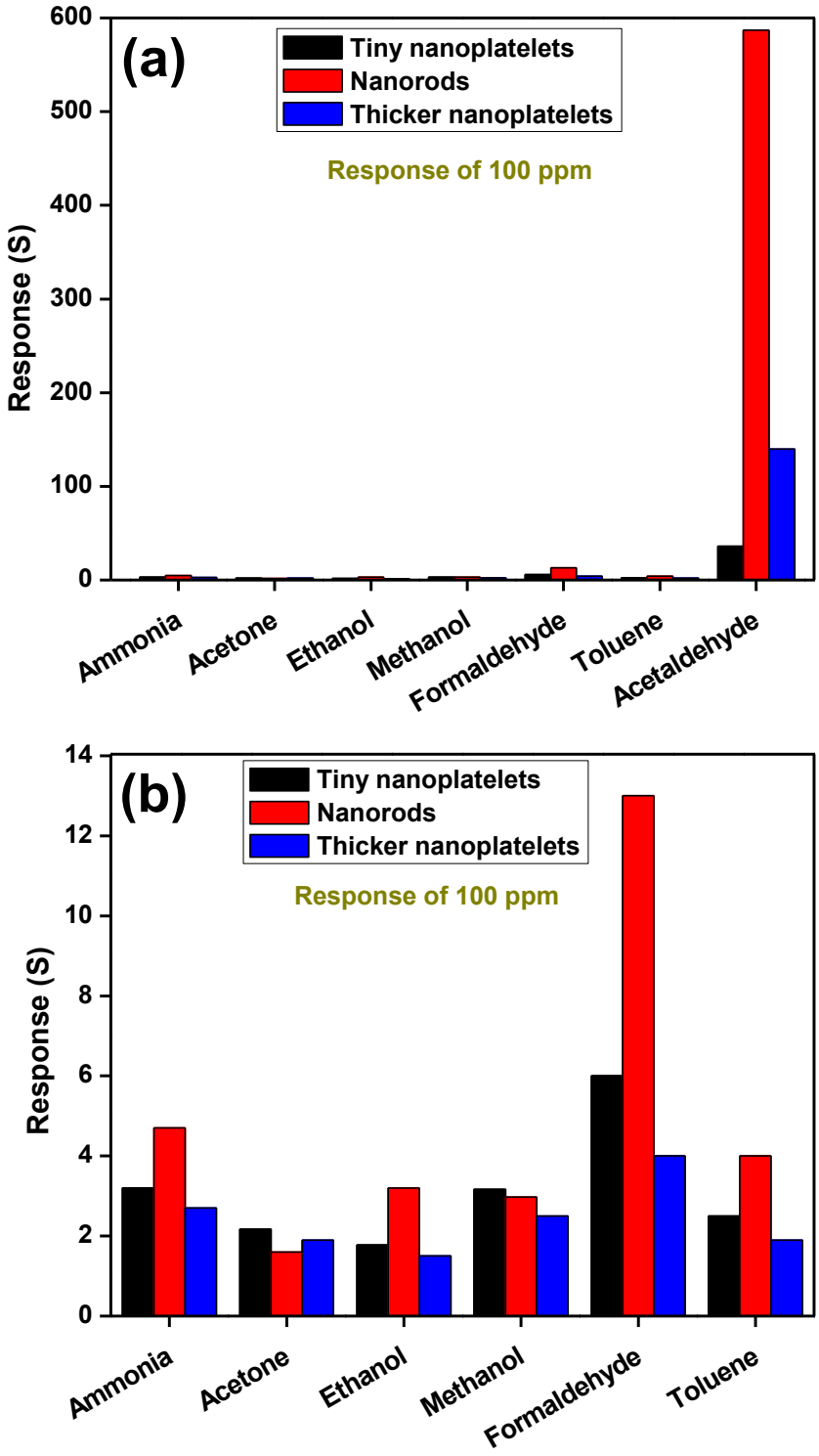

RSC Advances Accepted Manuscript

Fig. 7

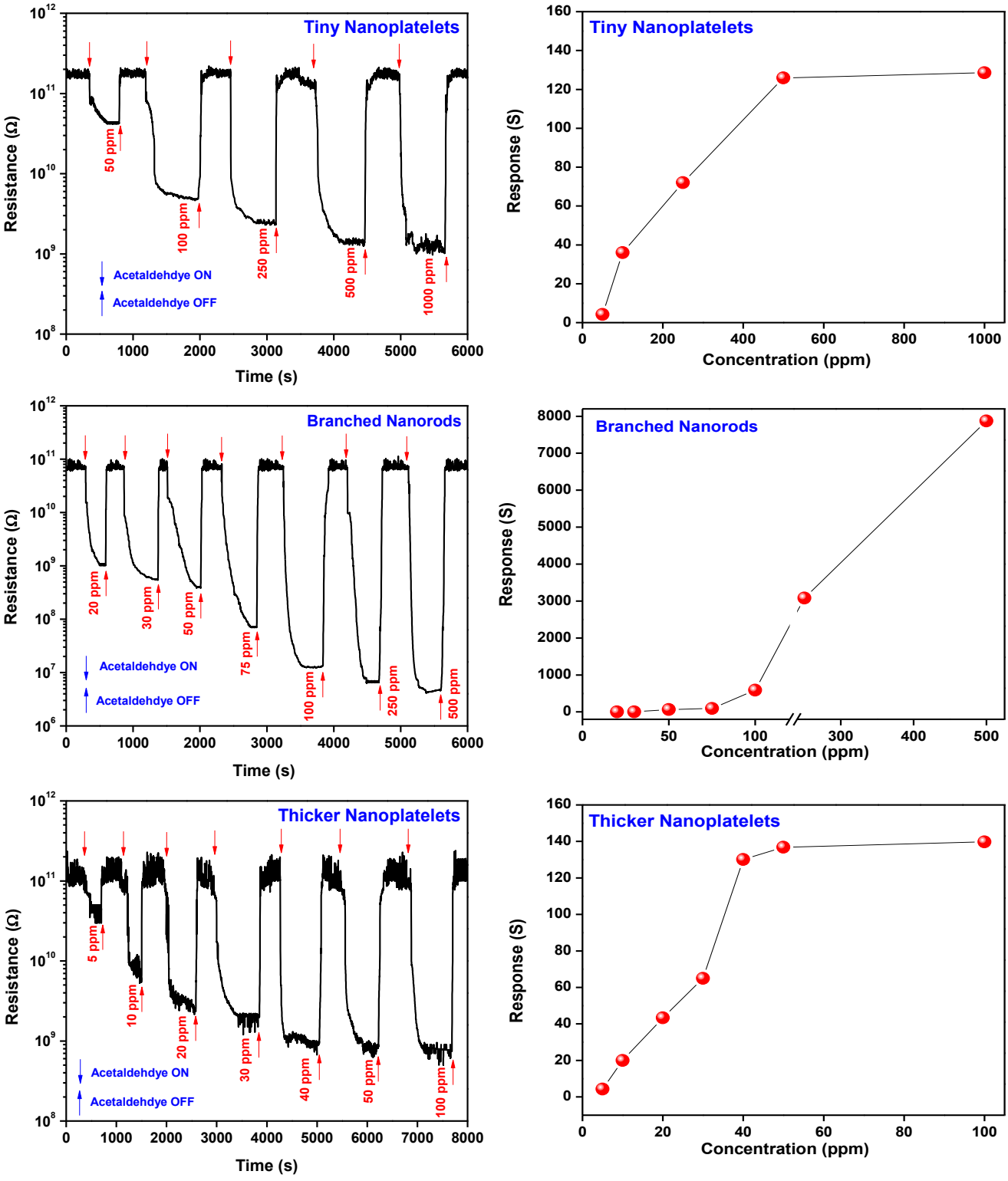

RSC Advances Accepted Manuscript

Fig. 8

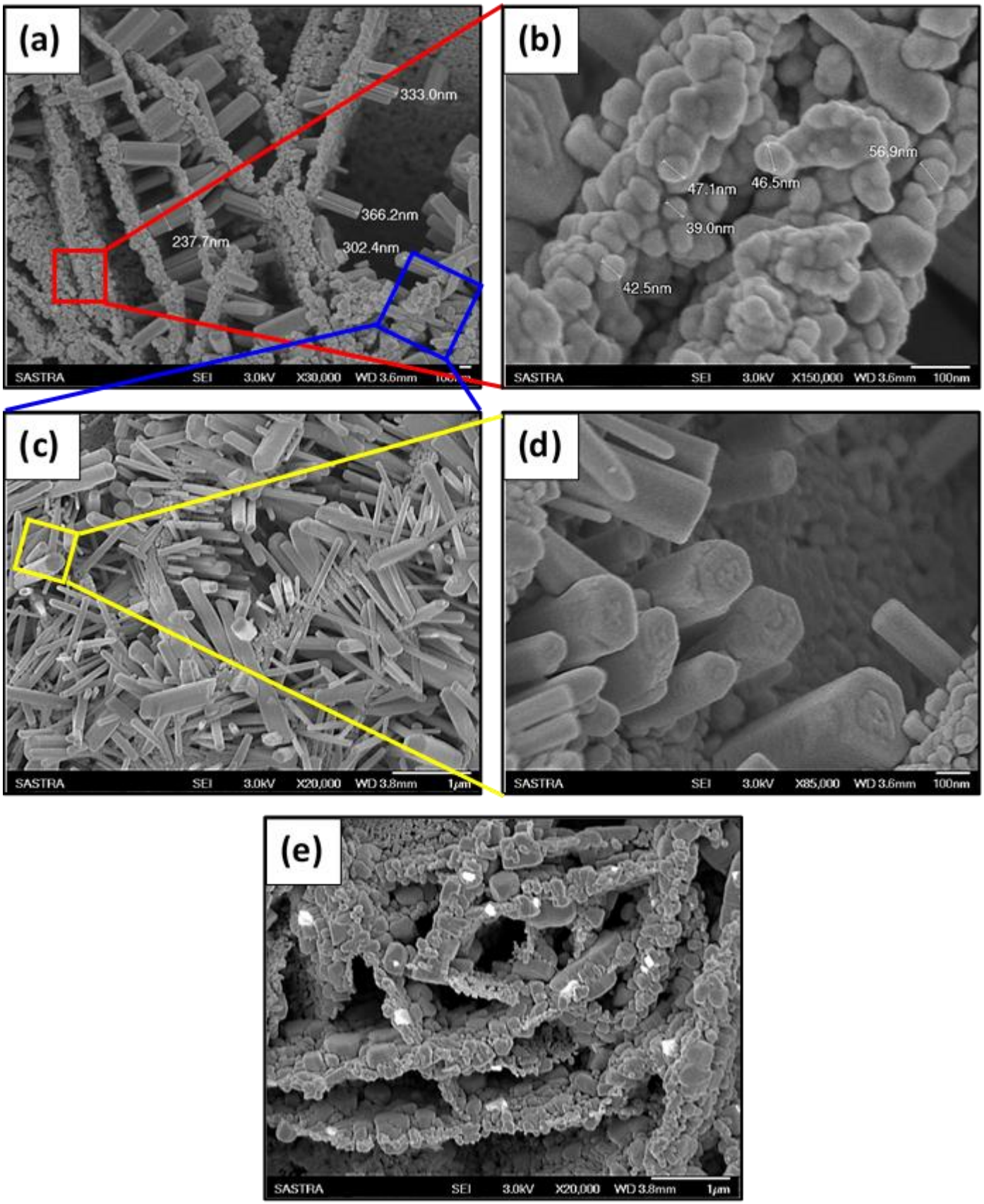

RSC Advances Accepted Manuscript

Fig. 9

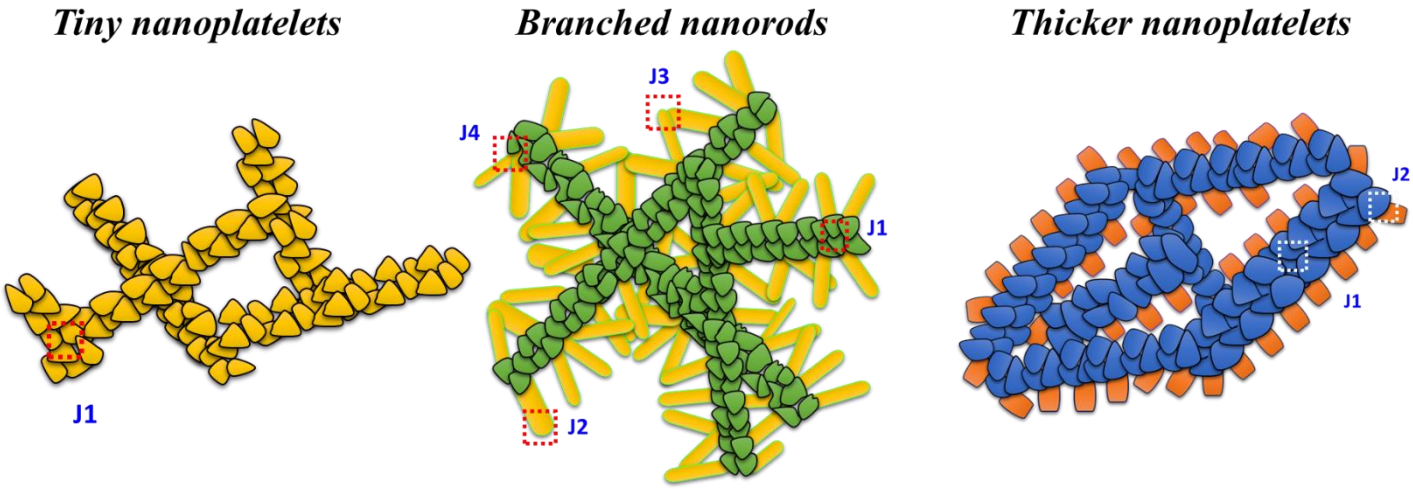

$J_{Total} = J1$ $J_{Total} = J1+J2+J3+J4$ $J_{Total} = J1+J2$

RSC Advances Accepted Manuscript

Fig. 10

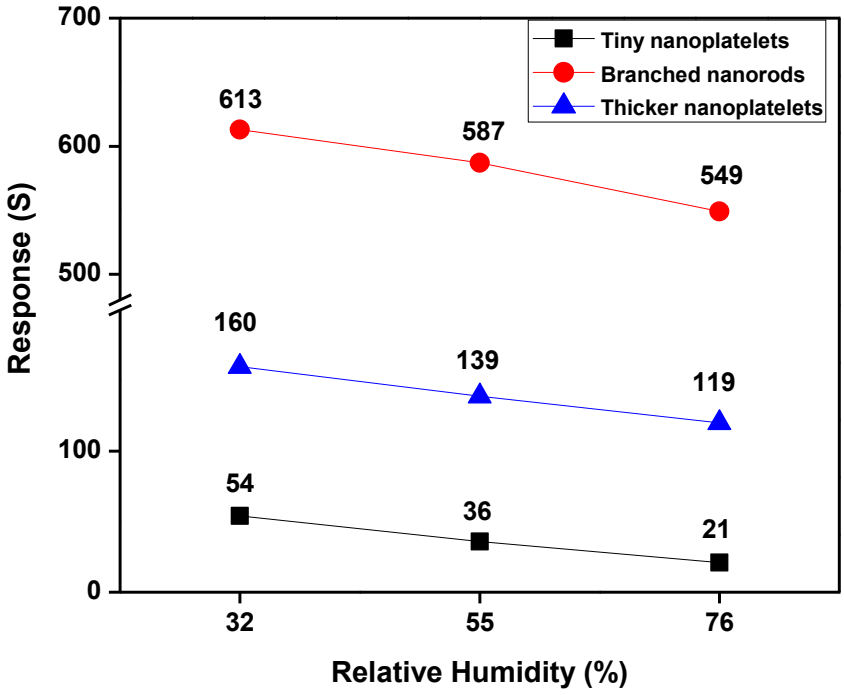

RSC Advances Accepted Manuscript